Construction and Building Materials 415 (2024) 134994

Contents lists available at ScienceDirect

Construction and Building Materials

journal homepage: www.elsevier.com/locate/conbuildmat

Mechanical behavior of construction and demolition waste-based alkali activated materials exposed to fire conditions

Ioanna Giannopoulou [a,*], Ponsian M. Robert [a,b], Michael F. Petrou [c], Demetris Nicolaides [a,b]

[a] Frederick Research Center, 7 Filokyprou Str. Pallouriotisa, Nicosia 1036, Cyprus
[b] Frederick University, Department of Civil Engineering, 7 Y. Frederickou Str. Pallouriotisa, Nicosia 1036, Cyprus
[c] University of Cyprus, Department of Civil & Environmental Engineering, 75 Kallipoleos Av., P.O. Box 20537, Nicosia 1678, Cyprus

ARTICLE INFO

Keywords:
Alkali activated materials
Geopolymers
CDW recycling
Elevated temperatures
Fire resistance
Compressive deformation

ABSTRACT

The mechanical behavior of materials based on the alkali activation of construction and demolition waste during and after their exposure to high temperatures was studied. The studied materials were based entirely on either, waste bricks or waste ceramic tiles, while a potassium hydroxide / sodium silicate solution was used as alkali activator. The compressive deformation of the alkali activated materials was tested during exposure to 850 - 1050 °C (on-fire testing) and the residual compressive strength was measured after exposure to 600 - 1050 °C for 2 h (post-fire testing), simulating the standard ISO 834 time-temperature curve. Microstructural changes and bulk properties were also assessed. The experimental results showed similar behavior of both materials in post-fire tests. Their compressive strength declined in between 600 and 800 °C and rose at 1050 °C, exceeding the initial value. Their density decreased 8 - 9% at 1050 °C, while their mass loss was 7 - 10% at this temperature. In the on-fire tests, the waste ceramic tile-based material presented plastic strain without any obvious macro-fracture at all the temperatures tested, while the waste brick-based material retained its elasticity and behaved as ceramic material up to 1000 °C with obvious macro-fractures. According to the experimental results, both alkali activated materials have the potential to be used as fire-resistant building materials.

1. Introduction

Cement-based concrete is today the most used material in the building industry worldwide, due to the excellent mechanical properties and durability in various environments. Although concrete is a non-combustible material with inherent fire resistance [1], when exposed to the high and rapidly rising temperatures experienced in a building fire, it suffers severe spalling, which occurs by breaking-off layers or chunks from the surface of the structural elements [1]. This phenomenon takes place at temperatures between 300 and 450 °C [2] and usually leads to heavy damages or even collapse of the structure, with all the obvious consequences for human life and property. Spalling of concrete is strongly related to the thermal transformation of the different phases, existing in Portland cement. The calcium-silicate hydrate (C-S-H) phase starts dehydrating at temperature around 200 °C [2] and is completely dehydrated over 750 °C [2,3]. Calcium hydroxide (portlandite) decomposes to calcium oxide at around 450 °C, while calcium carbonate (calcite) decomposes to calcium oxide at above 750 °C; the formed calcium oxide starts melting at around 800 °C [4]. In general, the mechanical strength of Portland cement-based concrete begins to decrease importantly at temperatures beyond 400 °C and becomes negligible at temperatures higher than 800 °C, without been recovered after cooling [3,4].

In recent years, the alkali activated materials, as well as the geopolymers and ionic polymers, have gained considerable attention as possible alternative binders to cement in the construction industry. These materials are formed through the activation of solid materials rich in silicate and/or aluminosilicate reactive phases, with alkali metal silicate solutions under highly alkaline conditions and at relatively low temperatures, usually below 100 °C [5]. Alkali activation involves a sequence of chemical reactions that give rise to the development of a partially or fully amorphous polymeric structure (network), consisting of the molecular units (or chemical groups) Si–O–Si and/or Si–O–Al [6,7]. The resulted materials generally possess excellent physicochemical, mechanical and thermal properties, such as micro- or nano-porosity, low water absorption and permeability, chemical and fire resistance, high mechanical strength, negligible shrinkage and low thermal expansion at high temperatures (up to 800 °C) [8–12]. Due to these properties, the

* Correspondence to: Frederick Research Center, 7 Filokyprou Str., Nicosia 1036, Cyprus.
E-mail address: ioangian@outlook.com (I. Giannopoulou).

https://doi.org/10.1016/j.conbuildmat.2024.134994
Received 13 August 2023; Received in revised form 31 December 2023; Accepted 10 January 2024

alkali activated materials are suitable for various applications in the building and construction industry, as ceramics, binders, coatings, etc. [8,11,13–18]. The research findings that are published to date on the fire resistance of alkali activated materials, geopolymers and inorganic polymers and their mechanical performance at elevated temperatures are promising. These materials behave much better than Portland cement at around 600 - 800 °C, while in most cases and even at temperatures higher than 800 °C, their compressive strength rises after cooling back at ambient temperature [19–21]. Relevant studies reported the thermal stability of metakaolin-based geopolymers, when they were properly cured so as to retain the amorphous structure up to their melting temperature [22], or when proper molar ratios Si/Al were selected so as to promote the formation of specific crystalline phases with high melting points [23]. As it is noted, the amount of crystalline phases formed in the alkali activated materials at high temperatures decreased with the increase of Si/Al ratio, regardless the alkali cation existing in the system (Na, K or Na-K) [24], while uncomplete crystallization of the amorphous polymeric phase reduced the mechanical strength of the obtained materials [16]. Regarding the type of alkali cation, it was observed that the potassium-based geopolymers showed minimum thermal deformation at elevated temperatures, followed by those based on sodium and potassium and then, by those based on sodium [25]. In addition, the mechanical and thermal properties of alkali activated materials at elevated temperature were strongly affected from the total alkali content in the alkali activating system [26]. The alkali activated materials based on metakaolin or fly ash (or on their mixtures) presented a rapid decline of the residual compressive strength after exposed at 800 °C, while the relevant specimens presented shrinkage cracking but no spalling phenomena, which are both mostly related to the increase of the average pore size [13,22–25,27]. In opposite, the compressive strength of the alkali activated materials based on granulated Ca-rich blast furnace slag (BFS) and exposed for 1 h to temperatures from 200 to 1000 °C, was constantly increased, achieving almost twice the initial value [30]. The BFS-based alkali activated materials were also proved fire-resistant materials, since after exposed to an 1100 °C flame, the back-side temperature was equilibrated to less than 400 °C after 35 min [18], which is enough time to evacuate a building in case of fire. Similarly, the materials based on the activation of electric arc furnace slag of ferronickel production with potassium hydroxide and silicate solutions presented excellent fire resistance, when tested according to the RWS temperature-time curve and proved able to withstand successfully a fire under such severe conditions [31]. Combinations of fly ash and slag in different ratios were also used to prepare alkali activated materials that were exposed at high temperatures, up to 800 °C [32]. The residual strength of the obtained materials decreased exponentially as their initial strength was increased and this behavior was attributed to the decreased of the specimens' ductility observed with the increase of the initial compressive strength.

The mostly studied waste sources for the development of fire-resistant alkali activated materials, geopolymers and inorganic polymers are the fly ash generated in thermal power plants and the slags of ferrous industry. Nowadays, the large volumes of the Construction and Demolition Waste (CDW) produced every year in industrialized countries make challenging their investigation as precursors for alkali activated materials [12,20,21,33–37]. In European Union (EU), around 450–550 million tons of CDW is produced every year, accounting for more than a third of the total industrial waste volume generated per annum [38]. The CDW is refers to the waste produced during the construction, renovation and demolition of buildings and infrastructure and it contains a wide variety of materials such as concrete, bricks, glass, metals, wood and asphalt. As is estimated, approximately 12% of CDW is concrete, while more than 54% corresponds to ceramic-type materials, i.e. bricks and tiles [33]. During the last decades, extensive research has been carried out for the recycling of CDW in the production of eco-friendly concrete, which can significantly reduce GHG emissions and save energy and the natural resources [39].

The present experimental study investigates the development of alkali activated materials based entirely on CDW, either waste bricks or waste ceramic tiles, to be used for the passive fire protection of buildings. More precisely, the mechanical behavior of the waste brick- and waste ceramic tile-based alkali activated materials during and after their exposure to high temperatures that occur in a fire is studied through appropriately designed tests. The studied alkali activated materials were evaluated in terms of physical and mechanical properties, while their microstructure has also been characterized by XRD and FTIR techniques, in order to better understand their behavior in fire conditions. The proposed approach for the CDW utilization brings maximum benefits for the environment through the sustainable recycling of secondary raw materials and the decrease of energy demand and CO_2 emissions, as well as for the economy, through a new low-cost processing route to produce materials for the effective passive fire protection of buildings. According to the results, the recycling of CDW in the production of fire-resistant alkali activated materials for buildings and construction applications is very promising.

2. Experimental

2.1. Materials

The brick waste (BW) and ceramic tile waste (CTW) used as precursors for the alkali activated materials developed in this study were received by the recycling company "Resource Recovery Cyprus-RRC", in Cyprus. Prior to their application, both the waste materials were milled and sieved to a particle size below 250 μm. According to the performed particle sized distribution analysis (Mastersizer S, Malvern Instruments), the mean particle diameter of BW was $d_{50} = 35.35$ μm and that of CTW was $d_{50} = 48.34$ μm. Table 1 presents the chemical composition of BW and CTW, as determined by X-ray fluorescence spectrometry (XRF-ED spectrometer, SPECTRO XEPOS). As shown in Table 1, both BW and CTW are siliceous materials with high content of aluminum and iron oxides. A high content of calcium oxide was also identified in the BW sample.

The bulk density and water absorption of the BW and CTW materials were determined according to the ASTM 128–88. The bulk densities of BW and CTW were almost similar and equal to 1.63 g/cm^3 and 1.82 g/cm^3, respectively. The water absorption of BW was 25.57%, while that of the CTW was importantly lower and equal to 15.77%.

The mineralogical analysis of the WB and WCT samples was performed by X-Ray diffraction method (XRD diffractometer, D8 Bruker; CuKα radiation, λ = 1.5418 nm) in the range of 2theta between 2° and 70°, with a scanning speed of 2° / min, and the results are presented in Figs. 1 and 2, respectively. As shown in Fig. 1, the main mineralogical phases found in the BW sample were quartz (SiO_2) and feldspars (anorthite-$CaAl_2Si_2O_8$ and albite-$NaAlSi_3O_8$), while calcite ($CaCO_3$) and hematite (Fe_2O_3) were also identified as secondary phases and diopside ($MgO{\cdot}CaO{\cdot}2SiO_2$), wuestite (FeO) and mullite ($3Al_2O_3{\cdot}2SiO_2$), as minor phases. According to the mineralogical analysis of the CTW sample (Fig. 2), quartz (SiO_2) was the predominant crystalline constituent with

Table 1
Chemical analysis of BW and CTW.

Oxides	BW	CTW
	mass, %wt.	
SiO_2	53.57	62.4
Al_2O_3	14.33	14.68
CaO	7.71	1.48
FeO	10.19	8.58
K_2O	3.74	3.76
MgO	4.07	3.68
Na_2O	0.66	0.98
TiO_2	1.46	-
Other	4.27	4.44

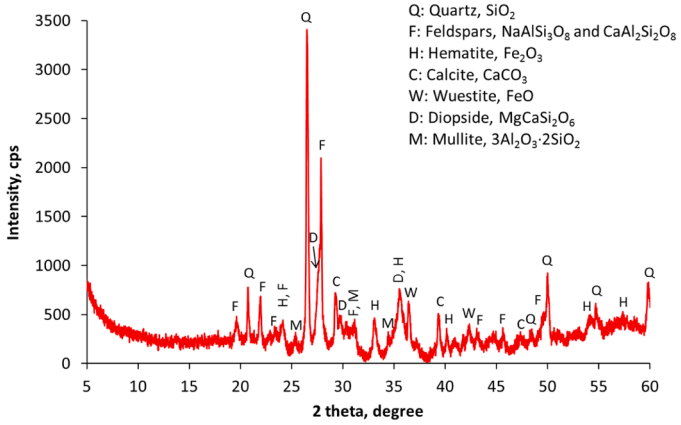

Fig. 1. XRD analysis of brick waste sample (BW).

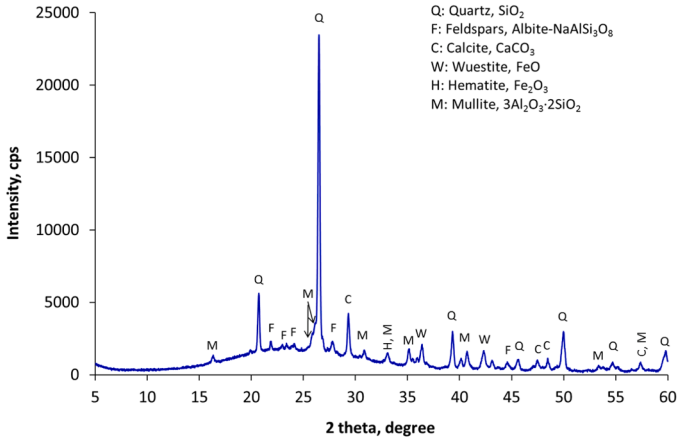

Fig. 2. XRD analysis of ceramic tile waste sample (CTW).

Na-feldspars (albite-$NaAlSi_3O_8$), calcite ($CaCO_3$), hematite (Fe_2O_3), wuestite (FeO), and mullite ($3Al_2O_3{\cdot}2SiO_2$) to contribute as minor phases. Except for the crystalline phases, an extended amorphous phase was also assigned to the CTW sample, as indicated by the broad hump registered in 2theta range between 18° and 32° (Fig. 2). It concerns for an amorphous aluminosilicate phase, which is also found in several raw materials used in alkali activated materials, such as metakaoline, fly ash and slag [40,41]. The existence of the amorphous Al-Si phase in CTW is strong evidence of this sample's suitability to be used as precursor for alkali activated materials.

The alkaline activator used in this work was prepared by mixing a potassium hydroxide (KOH) solution of 8 M with a sodium silicate solution (MERCK, $Na_2O = 8\%$, $SiO_2 = 27\%$, $H_2O = 65\%$ and $d = 1.346$ g/mL) under a constant volume ratio (Table 2). The KOH solution was prepared by dissolving pellets of analytical grade anhydrous potassium hydroxide (MERCK, 99.5% purity) in distilled water. The concentration of the formed KOH solution was constant in all the experiments and equal to 8 mol/L (8 M).

2.2. Preparation of the alkali activated materials

Two alkali activated materials were studied in this work: one of them was based on brick waste (BFR) and the other one, on the ceramic tile waste (CTFR). Table 2 summarizes the ratios of the main components used in their synthesis. The quantities of solid precursors and alkaline solutions shown in Table 2 have been standardized for a three-cell mold of cubic specimens with 50 × 50 × 50 mm dimensions.

Alkali activated materials were prepared by mixing the solid precursor, either WB or WCT, with the alkaline activator in a Hobart mixer for 5 min to form a homogeneous and viscous paste. The paste was then casted into steel cubic molds of 50×50×50 mm dimensions and cured in open molds for 7 days at 50 °C, under conditions of atmospheric pressure and non-controllable humidity. After curing, the specimens of the produced alkali activated materials were demolded and stored at ambient conditions, before any analysis and test being performed.

2.3. Analyses and testing procedures

The chemical analysis of the starting materials was performed by the X-Ray Fluorescence method, using a SPECTRO Xepos ED-XRF spectrometer. The mineralogical analysis of the starting and the produced materials was performed by the X-Ray Diffraction (XRD) method, using a D8 Bruker diffractometer (CuKα radiation, λ = 1.5418 Å with tungsten filament at 40 kV and 30 mA), in the range 2θ from 2° to 60° with scanning rate of 2° / min. The microstructural analysis of the alkali activated materials was studied with the Fourier Transform Infra-Red (FTIR) method, using a Perkin Elmer 2000 spectrometer. The infrared spectra recorded in the wave number range from 650 to 4000 cm^{-1} were collected in the atmosphere, using the Attenuated Total Reflection (ATR) technique with a Zn/Se crystal.

The uniaxial compressive strength of the alkali activated materials was determined with a 2000 kN electro-hydraulic mechanical loading machine. The as-cured specimens were tested after 7 days curing and 28 days hardening time, whereas the specimens exposed to high temperatures were tested immediately after their cooling back to room temperature. The stated values of compressive strength in both cases are the average of three cubic specimens' measurements. These cubic specimens were also used to measure the mass loss at the elevated temperatures, as well as to determine the materials density, as the ratio of their mass to volume. The mass loss and density results reported are the average of three measurements.

In this study, two different testing procedures were used to investigate the mechanical behavior of the produced alkali activated materials at elevated temperatures: during their exposure (on-fire testing) and after their exposure (post-fire testing). The on-fire tests of the alkali activated materials were performed at the National Centre for Scientific Research "DEMOKRITOS" (Athens, Greece), while the post-fire tests took place at the Frederick Research Centre (Nicosia, Cyprus).

In the on-fire tests, three cylindrical specimens of each alkali activated material were tested at three different temperatures. The specimens had nominal diameter 12 mm and height 16 mm and were selected among 10 specimens cut with diamond pot-saws from a single block of each alkali activated material with dimensions 100 × 100×20 mm to ensure sample uniformity. The blocks of the alkali activated materials were cured for 7 days at 50 °C and hardened for 7

Table 2
Synthesis conditions of the CDW-based alkali activated materials.

Code name	Precursor (g)		Alkaline Activator					S/L (g/mL)
			Solutions (mL)		*Volume Ratios*	*Molar Ratios*		
	WB	WT	KOH	Na_2SiO_3	$Na_2SiO_3{\cdot}H_2O$/KOH	H_2O/K_2O	SiO_2/K_2O	
BFR	2720	-	418	670	1.6: 1.0	20.5: 1	2.4: 1.0	2.5
CTFR	-	2500	283	452	1.6: 1.0	10.7: 1	1.2: 1.0	3.4

days at ambient conditions, before cutting the cylindrical specimens. Testing was performed on an Instron 5982 testing frame (100 kN load cell) equipped with a high temperature furnace capable to reach over 1300 °C (Fig. 3a). Each specimen was compressed, using an arrangement of alumina rods fitted with silicon carbide (SiC) platens. For purposes of protection and self-alignment, alumina/silica foam insulation was used between the SiC platens and the specimen, except for the tests performed at temperatures 1000 °C and above, where stainless steel slims were used. The CTFR alkali activated material was tested at the temperatures of 850, 950 and 1050 °C, while the temperatures of 950, 1000 and 1050 °C were selected for testing the BFR alkali activated material. A heating rate between 300 - 400 °C/h and a displacement rate of 500 mm/min were applied in all tests. The temperature precision throughout each test was 5 °C.

In the post-fire testing of the alkali activated materials, a muffle furnace was used (Fig. 3b). The investigated materials were heated to three different temperatures, 600, 800 and 1050 °C for 2 h, simulating thus the conditions of the standard ISO 834 time-temperature curve. The structural integrity of the materials was evaluated after the tests, in terms of residual compressive strength, mass loss and density. Three cubic specimens of 50 mm edge of each alkali activated material, which were cured for 7 days at 50 °C and hardened for 7 days at ambient conditions, were fired at each temperature. In each test, the specimens were put in the furnace, which started operating with a heating rate of 4.4 °C / min to reach the pre-defined temperature. When the desired temperature was reached, the specimens left in the furnace for 2 h and then, they were removed from the furnace and allowed to cool back to room temperature in open air conditions, before the performance of any test and measurement.

3. Results and discussion

3.1. Alkali activation of brick- and ceramic tile-waste

The alkali activation of brick waste and ceramic tile waste used as raw materials in this study was investigated it terms of mechanical strength and structural transformations occurred after their curing and hardening. Fig. 4 presents the compressive strength of BFR and CTFR alkali activated materials, after curing at 50 °C for 7 days and hardening at ambient conditions for 7 and 28 days. Both BFR and CTFR materials developed significant compressive strength, which is a strong indication

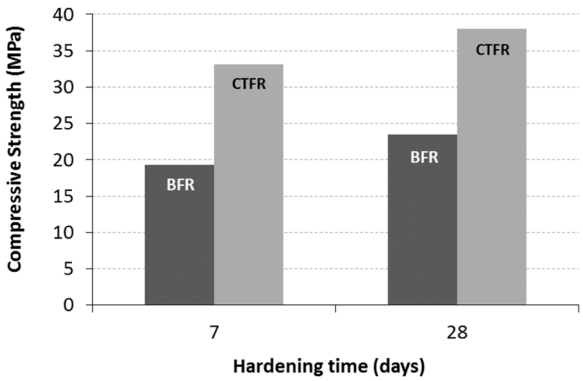

Fig. 4. Compressive strength of BFR and CTFR alkali activated materials hardened for 7 or 28 days, at ambient conditions (curing at 50 °C for 7 days).

of the successful alkali activation of brick waste (BW) and ceramic tile waste (CTW). As shown in Fig. 4, the compressive strength of CTFR was higher than that of BFR, regardless of the hardening time, while for both alkali activated materials, the increase of hardening time favored the development of compressive strength. More precisely, the compressive strength of BFR and CTFR after 7 days hardening was about 19 and 33 MPa, respectively, while after 28 days hardening, it was 23 and 38 MPa, respectively. Therefore, the compressive strength was increased only by 21% for the BFR and 15% for the CTFR materials after three weeks, which confirms the unique property of the alkali activated materials to develop high early mechanical strength.

The mechanical strength of the alkali activated materials is related to the alkali-aluminum-silicate phase formed in them, as well as the hardness of the minerals existing in the raw materials. In Fig. 5, the XRD patterns of BW and the derived alkali activated material BFR are presented. As shown in Fig. 5, all crystalline phases primarily presented in the BW were also identified in the XRD pattern of the BFR. However, some of them, like calcite, were importantly declined in BFR. Besides, new phases were also detected in BFR. The broad hump registered in the 2theta range from 14° to 21° in the XRD pattern of BFR (Fig. 5b) is characteristic of amorphous aluminosilicate precipitants [29,42,43] and was attributed to the (Na,K)-Al-Si phase formed in the BFR alkali activated material, while a new crystalline phase appeared at 2theta about 34° (main peak) was attributed to the potassium-based aluminosilicate

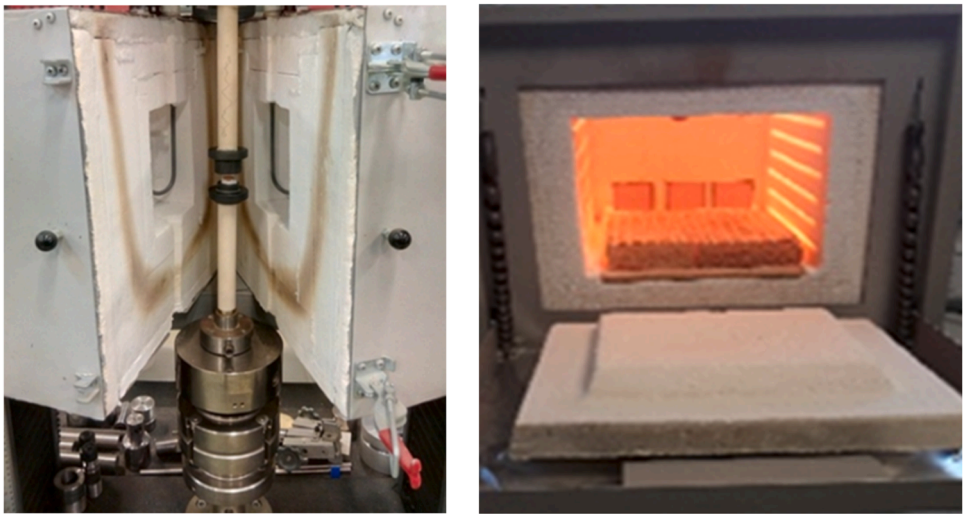

(a) (b)

Fig. 3. (a) Arrangement for the on-fire testing of the alkali activated materials in the Instron 5982 loading frame and furnace and (b) maffle furnace used for the post-fire testing of the materials.

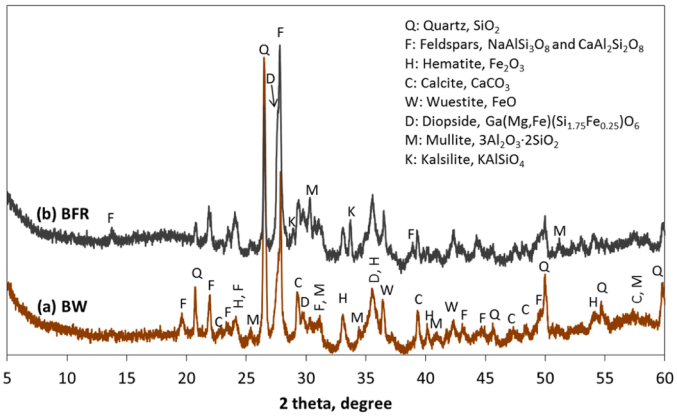

Fig. 5. XRD patterns of brick waste (BW) and the derived alkali activated material (BFR).

mineral kalsilite ($KAlSiO_4$). Both these new phases detected in the XRD pattern of BFR provide strong evidence for the alkali activation and a partial polymerization of the BW, which occurs through the dissolution of the BW aluminosilicate phases, most probably of the feldspars that dissolve in alkaline solutions [44] and the Al and Si combination with the alkalis K and Na that exist in the used activating solution.

The disappearance of the calcite peak and the formation of kalsilite, as new crystalline phase, were also observed in the XRD pattern of the CTFR alkali activated material (Fig. 6). In addition, the extended broad hump that was registered in 2theta between 20° and 30° in the XRD pattern of CTW (Fig. 6a) and assigned to an amorphous aluminosilicate phase, was slightly shifted toward higher values of 2theta, from 22° to 35°, in the XRD patterns of the CTFR (Fig. 6b), indicating partial dissolution of the primarily present aluminosilicate phase and formation of a new one [29]. Since the dissolution of amorphous Al-Si phases in alkaline solutions is faster and equilibrates almost immediately, in comparison to any crystalline phase in the same solutions [43,44], the formation of the (Na,K)-aluminosilicate phase in CTFR occurred at a faster rate and to a greater extent from the early stages of the process than in BFR, enhancing thus the development of a higher mechanical strength. In addition, CTW consisted almost entirely of quartz (Fig. 2) that has a Mohs scale hardness ranging between 7.0 and 7.5, while BW contained a significant amount of feldspars, except for quartz (Fig. 1), which decreases the hardness of its particles since the feldspars hardness ranges between 6 and 6.5 on the Mohs scale. Therefore, the mineralogy of the solid precursors used in this study favors again the development of higher compressive strength in the CTFR alkali activated material.

The structural transformations, confirming the alkali activation and a partial polymerization of the waste raw materials and favoring the development of higher compressive strength in CTFR than in BFR material, were also revealed through FTIR analysis. In Fig. 7, the FTIR spectra of the waste raw materials and the derived alkali activated materials are presented. The spectra of the waste materials BW and CTW are illustrated in Fig. 7(a) and (c), respectively, while the spectra of the corresponding alkali activated materials, BFR and CTFR, are given in Fig. 7(b) and (d), respectively.

The broad and the relatively intense bands identified at the wavenumbers 1450 cm^{-1} and 877 cm^{-1}, respectively, in the FTIR spectra of both the waste materials (BW and CTW) were attributed to stretching and bending vibrations of the C-O bond, indicating the existence of carbonate phases in the initial raw materials (i.e. calcite, $CaCO_3$). In the FTIR spectra of the derived alkali activated materials BFR (Fig. 7b) and CTFR (Fig. 7d), a shifting of the peak at 1450 cm^{-1} to a higher wavenumber (1460 cm^{-1}) was observed, while the absorption band located at 877 cm^{-1} in both BW and CTW spectra was absent. These transformations indicated dissolution of the carbonate phases existing in the waste raw materials, through the alkali activation, and molecular rearrangement in the formed phases [35].

The wide absorption band observed at the wavenumbers 1010 and 1020 cm^{-1} in the spectra of BW (Fig. 7a) and CTW (Fig. 7c), respectively, was assigned to asymmetric stretching vibrations of the Si-O-*T* bonds (where *T* could be Si or Al) and comprises the fingerprint of Al-Si polymerization [29,45,46]. This band shifted to lower wavenumbers in the spectra of the BFR (Fig. 7b) and CTFR (Fig. 7d) alkali activated materials and more precisely, at 978 cm^{-1} and 995 cm^{-1}, respectively. The displacement of this band to lower wavenumbers indicates dissolution of aluminosilicate phases present in the waste materials and Al-Si polymerization, during the alkali activation [21]. Moreover, the peak located at 995 cm^{-1} in the spectrum of CTFR (Fig. 7d) was more intensive and sharper than the respective peak appeared at 978 cm^{-1} in the spectrum of BFR (Fig. 7b). This difference reveals that the amorphous Al-Si polymeric phase formed in the CTFR material was more extensive and composed of highly polymerized species (trimers, rings, planes, etc.), which contained bridged rather than terminal Si-O bonds and chains of similar sizes. In opposite, the extent of the Al-Si polymeric phase formed in BFR material was limited and consisted of polymeric species of diverse chain sizes [14,45,46]. These observations comply with the compressive strength data given in Fig. 4, where the CTFR alkali activated material developed higher values (33 and 38 MPa, after hardening for 7 and 28 days, respectively) than the BFR one (19 and 23 MPa, after hardening for 7 and 28 days, respectively). Finally, the peak appeared at 850 cm^{-1} in FTIR spectra of the BFR (Fig. 7b) and CTFR (Fig. 7d) materials was ascribed to symmetric stretching vibrations of the Al-O bonds and constitutes an important sign of polymerization that is associated with the dissolution of Al-phases from the initial

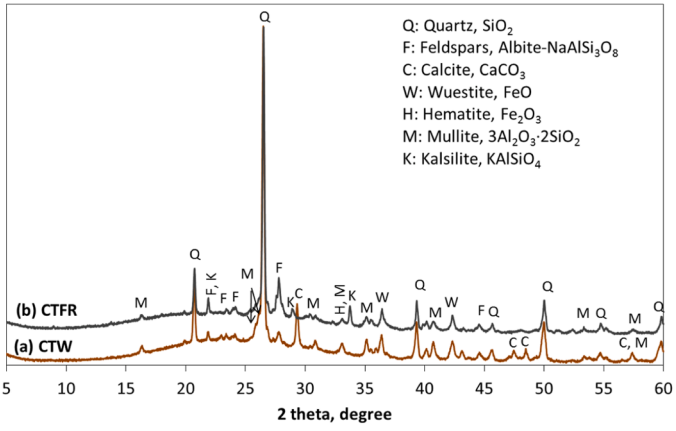

Fig. 6. XRD patterns of ceramic tile waste (CTW) and the derived alkali activated material (CTFR).

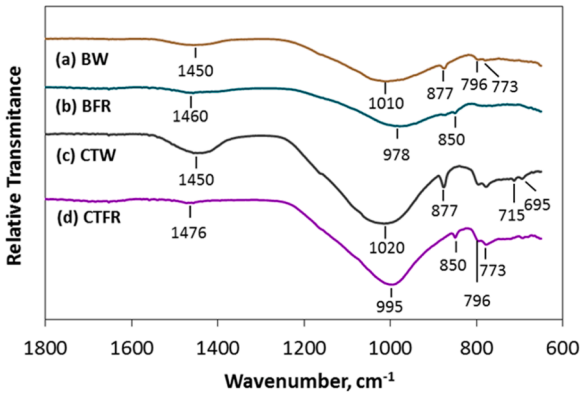

Fig. 7. FTIR spectra of (a) brick waste (BW), (b) brick waste-based alkali activated material (BFR), (c) ceramic tile waste (CTW) and (d) ceramic tile waste-based alkali activated material (CTFR).

solids through alkali activation and their rearrangement in the formed polymeric matrix [45,46]. The same indication also applies to the weak double band that was appeared at 773 cm^{-1} and 796 cm^{-1} in the spectra of both waste materials BW and CTW and decreased or disappeared in the spectra of the derived alkali activated materials BFR and CTFR, respectively, as well as to the weak double band located at 715 cm^{-1} and 695 cm^{-1} in CTW spectrum (Fig. 7c) and missed in the spectrum of the corresponding CTFR alkali activated material (Fig. 7d).

All the aforementioned observations are consistent with the development of a polymeric network in the BFR and CTFR materials, which constitutes the backbone of their structure. The higher polymerized Al-Si phase in CTFR and its well-ordered structure with the predominance of bridge Si-O over terminal Si-O bonds, in comparison to that of the BFR, justifies the development of higher compressive strength in the former material.

3.2. On-fire testing of alkali activated materials

The compressive deformation tests of the alkali activated materials at high temperatures were designed, in order to better understand their mechanical behavior in fire, under simultaneous load bearing. In Figs. 8 and 9, the engineering stress-strain curves of BFR and CTFR alkali activated materials, respectively, for the temperatures tested are presented. The engineering measurements of stress and strain denoted in Figs. 8 and 9 as σ_e and ε_e, respectively, are determined from the load applied and the resulted displacement, using the original specimen's cross-sectional area (A_0) and height (H_0), according to Eqs. (1) and (2), respectively.

$$\sigma_e = P/A_0 \tag{1}$$

$$\varepsilon_e = h/H_0 \tag{2}$$

where P, is the load applied; A_0, is the original specimen's cross-sectional area; h is the specimen's displacement and H_0 is the original specimen's height.

According to Fig. 8, stress is proportional to strain for the BFR alkali activated material at the temperature of 950 °C and partially proportional at 1000 °C, with the constant of proportionality being the modulus of elasticity or Young's modulus, denoted E (Eq. 3).

$$\sigma_e = E \quad \varepsilon_e \tag{3}$$

The linearity between stress and strain at 950 °C indicated elastic behavior for the BFR material, which is characteristic of brittle materials, like hard ceramics. As shown in Fig. 8, the stress - strain variation at this temperature was linear throughout the full range of strain values, eventually terminating in fracture without appreciable plastic flow. The

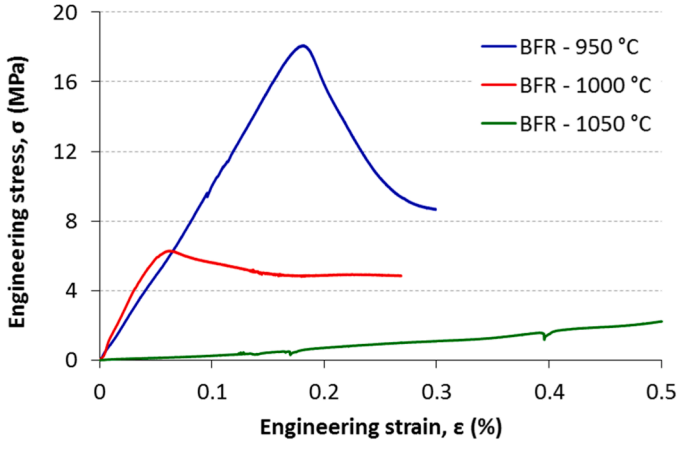

Fig. 8. Engineering stress-strain curve of BFR alkali activated material (on-fire testing).

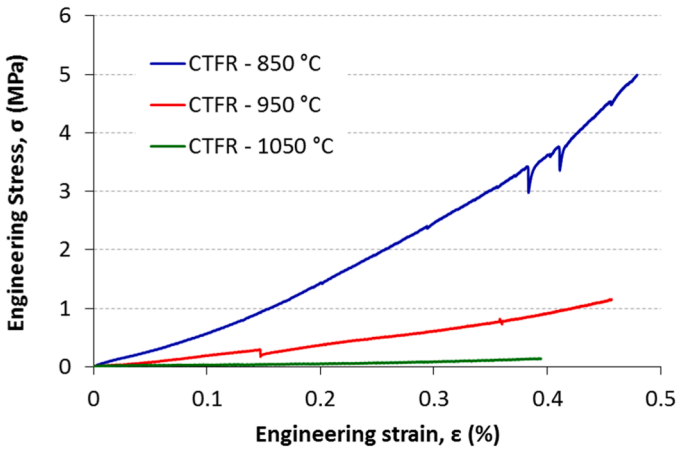

Fig. 9. Engineering stress-strain curve of CTFR alkali activated materials (on-fire testing).

stress yield was about 18 MPa, which is similar to the compressive strength of the BFR alkali activated material after curing and hardening for 7 days (19 MPa). At the temperature of 1000 °C, BFR still exhibited an elastic zone in the early portion of the stress-strain curve (Fig. 8), which was delimitated by a yield stress of about 6 MPa. After this initial stage, stress deviated from the linear proportionality with the increase of stain and the material underwent plastic deformation, exhibiting ductile behavior. At the highest tested temperature of 1050 °C, BFR behaved as a plastic material and the compression of the tested specimen was continued up to about 50% apparent strain (Fig. 8) without any obvious macro-fracture. The plastic behavior can be attributed to the melting of alkalis that occurs at temperatures above 800 - 900 °C [48] and forms with the non-molten constituents a plastic mass deformed by its own weight or an external load.

Regarding the CTFR alkali activated material, the stress-strain curves obtained at all tested temperatures (Fig. 9) were indicative of a plastic behavior with permanent deformation of the material. At the lowest tested temperature of 850 °C, a drastic decline of compressive strength was observed, which was approximately one-sixth of the value after curing and hardening for 7 days (from 33 MPa to about 5 MPa), while at temperatures above 850 °C, the CTFR material yielded negligible compressive strength (Fig. 9), exhibiting ductile behavior from the test starting. At all tested temperatures, the CTFR specimens' deformation was stopped at about 40–50% apparent strain, without any obvious macro-fracture.

In Figs. 10 and 11, the specimens of the BFR and CTFR alkali activated materials, respectively, before and after the on-fire tests conducted in the different temperatures, are illustrated. As shown in Fig. 10 (b), the BFR specimen presented brittle failure with nearly negligible deformation, during the test at 950 °C. At this temperature, plastic strain is generally absent (Fig. 8) and the scant energy is absorbed during failure, while the cracks formed under the applied load were unstable (Fig. 10b), meaning that they could continue to grow spontaneously, without increasing the load. The compressive strength of BFR specimen at 950 °C was about 18 MPa (Fig. 8), which means that the BFR alkali activated material can withstand a load of about 18 MPa in fire conditions without any deformation and recover its original shape, when this load stops applying. According to Fig. 10 (c), during the compression test at 1000 °C, the BFR material presented brittle failure behavior in the early stage of the test, but finally it exhibited ductile failure with permanent deformation delimitated by a yield stress of around 6 MPa (Fig. 8), which was approximately one-third of the material's compressive strength after curing and hardening for 7 days (Fig. 4). As seen in Fig. 10 (c), there were many heavy cracks formed on BFR specimen at the early stage of this test, tending to split it into two or more pieces. However, due to the presence of plastic strain in the

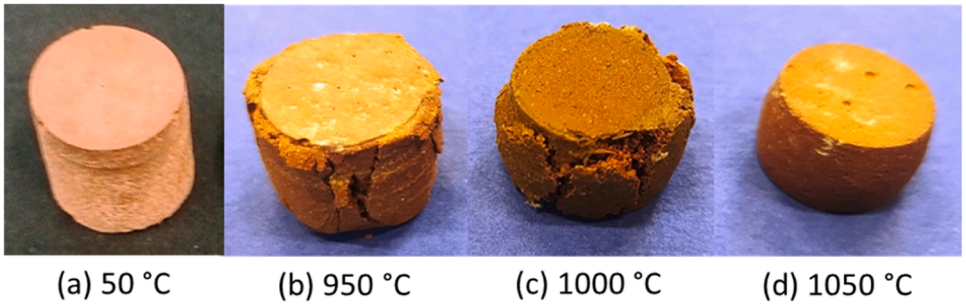

Fig. 10. BFR specimens after (a) curing and on-fire testing at (b) 950 °C, (c) 1000 °C and (d) 1050 °C.

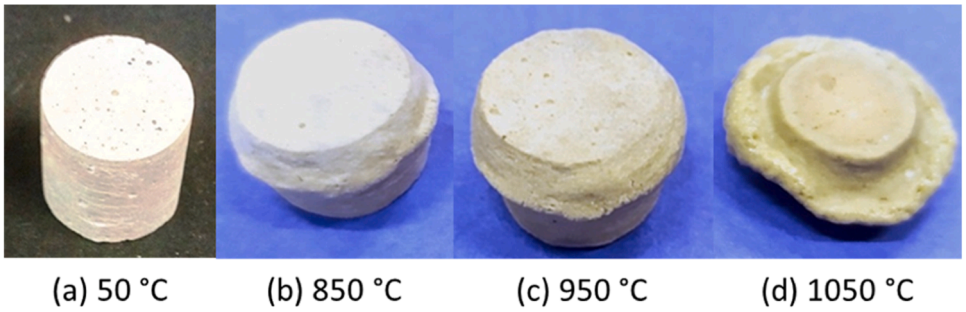

Fig. 11. CTFR specimens after (a) curing and on-fire testing at (b) 850 °C, (c) 950 °C and (d) 1050 °C.

following stages of the test at this temperature, the cracks propagation was constrained and the material eventually exhibited ductile failure.

At the highest tested temperature of 1050 °C, BFR alkali activated material exhibited plastic behavior and the specimen was deformed (flattened) without failing, taking finally a shape like a barrel (Fig. 10d). At this temperature, which is close to the melting point of sodium oxide (~1130 °C) and sodium silicates (~1080 °C), the formation of a pseudo-viscous phase in the alkali activated materials results in their softening and thus, their deformation in the presence of an even small load, but not (always) their breaking. The compression of the relevant specimen was continued up to about 50% strain (Fig. 8) without any obvious macro-fracture.

The color change from red to brownish red observed in the BFR specimens, before and after their submission to high temperature tests (Fig. 10), was associated with the phases transformation occurred at the tested temperatures. The high concentration of iron oxides in the BW (Table 1), in particular of hematite and wuestite (Fig. 1), was responsible for the red color of the BFR specimens before testing. During the firing tests, the formation of diopside at around 900 °C provided with a yellowish color the BFR specimens, favoring the development of the lighter color of brownish red [47].

In opposite to BFR, the CTFR alkali activated material exhibited plastic behavior at all tested temperatures (Fig. 11) and readily deformed above at least 850 °C without breaking. As shown in Fig. 11 (d), at the highest tested temperature of 1050 °C, CTFR specimen was totally deformed, while it was also softened due to melting, as indicated a slight yellowish change in color. Softening occurs in the alkali activated materials at temperatures above 900 °C, because certain constituents, usually alkali-phases, start melting at these temperatures, forming a pseudo-viscous phase that enhances a pseudo-plastic behavior. Signs of softening were also observed at the tested temperature of 950 °C (Fig. 11c). As seen in Fig. 11, the CTFR specimens were flattened without failing at all temperatures tested, developing very low or negligible compressive strength (Fig. 9).

3.3. Post-fire testing of alkali activated materials

In Fig. 12, the relative compressive strength of the BFR and CTFR alkali activated materials is presented, after their exposure to elevated temperatures for 2 h and immediate cooling back to ambient temperature. As shown in Fig. 12, the change of compressive strength with temperature followed similar trend for both of the alkali activated materials, with greater intensity in the case of CTFR material.

According to Fig. 12, BFR alkali activated material lost 20% of its compressive strength (~19 MPa), after its exposure to 600 °C. At 800 °C, the residual compressive strength of BFR was increased, reaching the initial value and slightly raised at the highest tested temperature of 1050 °C. In opposite, the residual compressive strength of CTFR alkali activated material declined abruptly to 50% and 40% of its initial value (~ 33 MPa), after being exposed to 600 and 800 °C, respectively (Fig. 12). At 1050 °C, the CTFR residual compressive strength was sharply increased, showing an improvement of about 10%

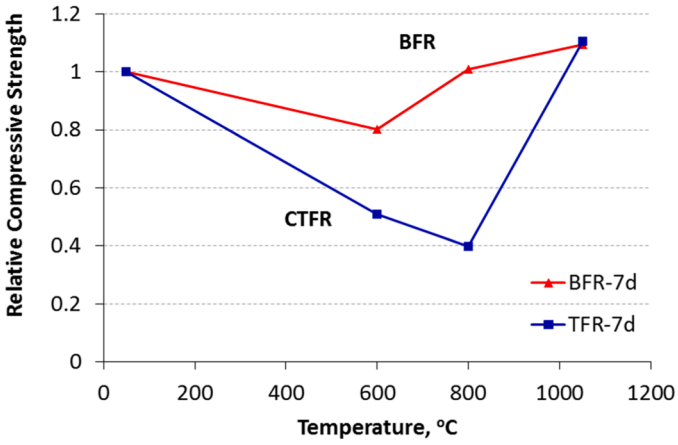

Fig. 12. Relative compressive strength of BFR and CTFR alkali activated materials after 2-h exposure to different temperatures (curing: 50 °C / 7 d; hardening: ambient temperature / 7 d).

compared to the initial value.

Despite that the compressive strength of CTFR was decreased by almost 60% after its exposure to 800 °C, it remained at 13 MPa, which is an acceptable value for building materials, when subjected to heat stress [31]. Similarly, after exposure at 600 °C, the BFR compressive strength remained at 15 MPa and therefore, both the CDW-based alkali activated materials developed in this study may be used for the passive fire protection of buildings and constructions.

The changes in the compressive strength of the alkali activated materials subjected to high temperatures heating is associated to important alterations and structural rearrangements occurred in the aluminosilicate phase (polymeric matrix) at these temperatures. During the heating of alkali activated materials at about 300 °C, the physically and chemically bonded water in the aluminosilicate phase evaporates gradually [46], while at temperatures above 300 °C and up to 550 °C, the dehydroxylation of silanol (>Si-OH) and aluminol (>Al-OH) groups is also carried out [5,48]. The dehydration and dehydroxylation of the aluminosilicate formed phase that occurred in the BFR and CTFR alkali activated materials up to 600 °C implied partial decomposition of the Si-O-Si and Al-O-Si bonds [35], disarranging thus the polymeric network and in turn, the structural integrity of materials. The formed vapour, in combination with the heat transfer, resulted in gradual growth in pore pressure inside the polymeric matrix and the development of micro-cracks that led to deterioration of the materials integrity and consequently, to significant reduction in their mechanical strength. Besides, the polymeric phase softening, due to the alkalis melting, which started at temperatures above 600 °C [28,48], also contributed to the decrease of materials compressive strength. At temperatures above 800 °C, alkalis act as fluxes and sintering phenomena are taking place (typically at temperatures around 50 – 80% of their melting point), which reduced the porosity and increased the bond area between the unreacted particle and thus, the strength of materials, leading to dense and durable structures [49,50]. Furthermore, certain mineralogical transformations that took place in the alkali activated materials at these temperatures, especially the disappearance of the amorphous phase and the enhancement and/or formation of crystalline phases, also affected their compressive strength.

The aforementioned structural changes that occurred in the studied alkali activated materials after their exposure to elevate temperatures, also affected their density and mass loss. The evolution of materials density and mass loss with temperature is presented in Figs. 13 and 14, respectively.

As shown in Fig. 13, the density of the CTFR alkali activated material was higher than that of BFR at all the tested temperatures, although the density of CTW was lower than the one of BW (2.81 and 2.56 g/cm^3, respectively). After the exposure to 600 °C, the density of both alkali

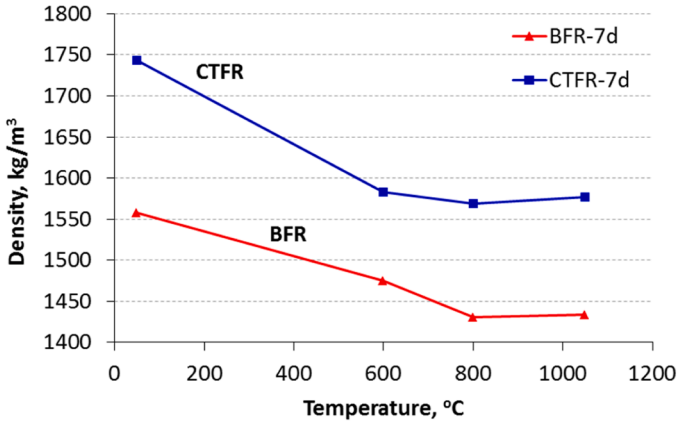

Fig. 13. Apparent density of BFR and CTFR alkali activated materials versus temperature, after 2-h exposure up to 1050 °C (curing: 50 °C / 7 d; hardening: ambient temperature / 7 d).

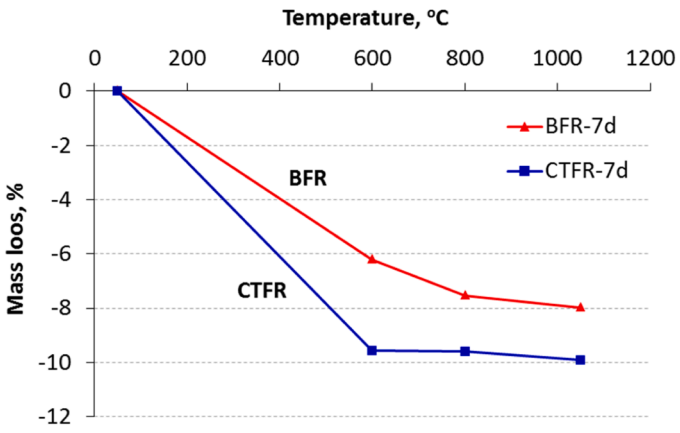

Fig. 14. Mass loss of BFR and CTFR alkali activated materials versus temperature after 2-h exposure up to 1050 °C (curing: 50 °C / 7 d; hardening: ambient temperature / 7 d).

activated materials was reduced, due to dehydration and dehydroxylation of the polymeric phase, which also involved the reduction of the materials' mass. According to Fig. 14, at 600 °C, BFR alkali activated material lost 78% of its total mass loss occurred up to 1050 °C and the CTFR material lost more than 96% of the total mass it had lost up to 1050 °C. The density of BFR alkali activated material continued to decrease up to 800 °C (Fig. 13), where it lost an additional 6% of its total mass loss. On the contrary, the CTFR material showed an almost constant density between 600 and 1050 °C (Fig. 13), as well as a constant mass loss (Fig. 14). However, above 800 °C, a slight density increase was observed for both alkali activated materials (Fig. 13), maybe due to shrinkage of the polymeric matrix that took place at above 850 – 900 °C [16,23].

The mechanical behavior of the investigated alkali activated materials in the post-fire tests was totally different from that in the on-fire tests. Especially at the highest tested temperature of 1050 °C, where both materials underwent plastic strain up to about 40–50% without failure during the on-fire tests (Figs. 10d and 11d), while during the post-fire tests, the compressive strength of both materials rose and exceeded by almost 10% the respective initial values. Actually, in the on-fire tests, BFR and CTFR alkali activated materials behaved similarly but not identically to ductile materials, which are known to normally undergo substantial plastic deformation with high energy adsorption prior to failure. This pseudo-plastic behavior of the investigated materials at 1050 °C would explain the increase of their compressive strength, after their exposure to elevated temperatures and cooling back to room temperature. The softening of the alkali-phases occurred at above 800 °C enhanced sintering phenomena that healed the cracking created due to the dehydration and dehydroxylation of the amorphous phase, constraining its spreading and propagation.

Only a few surface micro-cracks, without any other sign of spalling or deformation, were visible on the BFR specimens, after their exposure to 600 °C. This cracking was more intense at 800 °C, while after the BFR specimens exposure to 1050 °C, cracking was disappeared due to self-healing by the viscous polymeric phase formed at this temperature [28]. In the case of the CTFR alkali activated material, it exhibited minimal and insignificant surface micro-cracking only after its exposure to 800 °C, which appeared to be healed at 1050 °C.

3.4. Structural transformations at high temperatures

The mineralogical transformations occurred in the investigated alkali activated materials after their exposure to elevate temperatures and cooling back to ambient temperature are summarized in Figs. 15 and 16, where the XRD patterns of BFR and CTFR materials, respectively, after being subjected to the post-fire tests are illustrated. The XRD patterns of

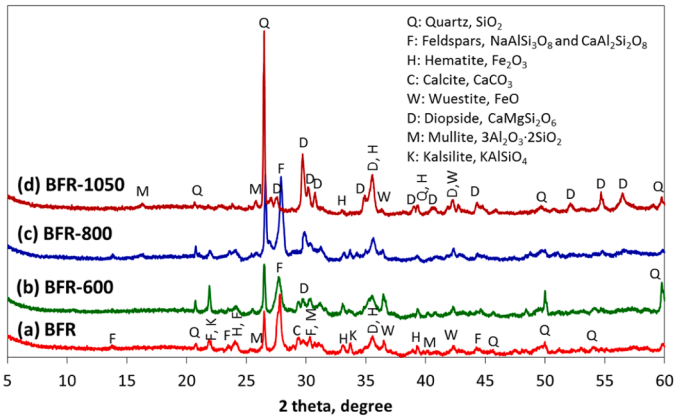

Fig. 15. XRD patterns of BFR alkaline activated material after (a) curing (50 °C / 7 d); (b), (c) and (d) 2-h exposure to 600 °C, 800 °C and 1050 °C, respectively.

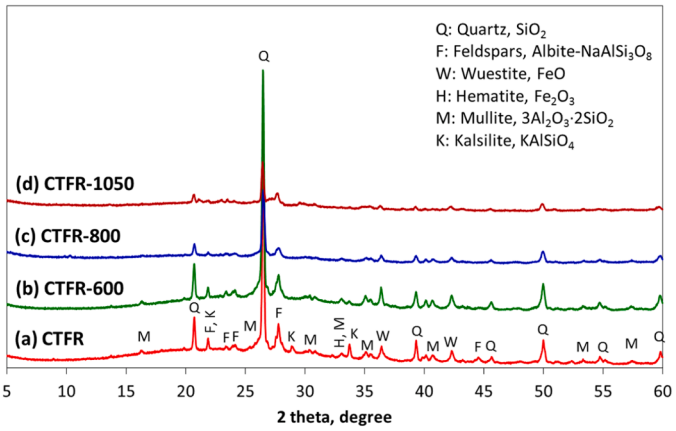

Fig. 16. XRD patterns of CTFR alkali activated material after (a) curing (50 °C / 7 d); (b), (c) and (d) 2-h exposure to 600 °C, 800 °C and 1050 °C, respectively.

the respective alkali activated materials after curing (50 °C / 7 d) are also included in Figs. 15 and 16, as control samples.

According to Fig. 15, no any difference was observed between the XRD patterns of the BFR specimen heated at 600 °C (Fig. 15b) and the non-heated one (Fig. 15a). After the exposure of BFR to 800 °C, important phases' transformations were observed with the disappearance of the broad halo peak registered in 2theta between 14° and 21° in the XRD pattern of BFR (Fig. 15a), which was associated to the amorphous phase and the slight increase of mullite and diopside peaks intensity. Finally, the BFR specimen heated to 1050 °C presented the most prominent mineralogical changes (Fig. 15d). Feldspars, which were dominant constituents in the BFR alkali activated material, were totally disappeared, as well as the newly formed phase of kalsilite, while the iron oxides hematite and wuestite detected in the XRD pattern of BFR material after curing (Fig. 15a) were importantly declined in intensity. In opposite, the crystalline phases of diopside and mullite were significantly increased in intensity and became dominant crystalline phase, along with quartz.

Similarly to BFR, the most important mineralogical transformations occurred in the CTFR alkali activated material were also observed in the XRD patterns of the specimens exposed to temperatures 800 °C and above. The broad halo that appeared in 2theta values from 20° to 35° in the XRD pattern of CTFR material after curing (Fig. 16a) was kept unchanged after its exposure to 600 °C (Fig. 16b), while declined significantly after its exposure to 800 °C (Fig. 16c) and almost disappeared at 1050 °C (Fig. 16d). Furthermore, except of quartz, the contribution of all the other crystalline phases detected in the CTFR alkali activated material, such as feldspars, iron oxides and mullite, was greatly reduced or minimized at 800 °C and above, where quartz dominated (Figs. 16c and 16d).

The disappearance of the amorphous phase formed in the BFR alkali activated material after curing and the enhancement of diopside and mullite crystallization occurred in BFR after its exposure to 800 °C and cooling back to ambient temperature, favored the mechanical strength of BFR (Fig. 12). Accordantly, the crystallization of the same amorphous phase occurred at 1050 °C in the case of CTFR alkali activated material, in combination with the sintering and densification, favored the development of high compressive strength at this temperature (Fig. 12).

The above-discussed microstructural changes that occurred in the studied alkali activated materials after their exposure to high temperatures, affecting their mechanical strength, were also revealed through the FTIR analysis. The FTIR spectra of BFR and CTFR alkali activated materials are presented in Figs. 17 and 18, respectively.

The most significant transformations are associated with the absorption band assigned to the stretching vibration of Si-O-*T* bonds. This band, which was located at 978 cm^{-1} in the spectrum of BFR (Fig. 17a), was moved to a lower wavenumber (939 cm^{-1}) after the exposure of BFR to 600 °C (Fig. 17b), indicating enhanced polymerization and moved again to a higher wavenumber (966 cm^{-1}), after the exposure of BFR to 800 °C (Fig. 9c), denoting recrystallization of the amorphous polymeric phase [16]. The above structural changes were consistent with the initial decrease and the subsequent increase of the compressive strength of BFR, after its exposure at 600 and 800 °C, respectively (Fig. 12). The same band became broader in the spectrum corresponding to the BFR specimen exposed to 1050 °C (Fig. 17d) and extended in the wavenumbers area from 1200 to 800 cm^{-1}, implying lower polymerized silica, which justifies the very small improvement in the compressive strength of the relevant material (Fig. 12).

Similarly, in the FTIR spectra of the CTFR alkali activated material, the absorption band of Si-O-*T* bonds stretching vibration that was located at 995 cm^{-1} before and after heating the material at 600 °C (Figs. 18a and 18b, respectively), was slightly shifted to higher wavenumbers after the exposure of CTFR at 800 and 1050 °C, as shown in Fig. 18 (c) and (d), respectively. This shifting indicated the sintering of the aluminosilicate amorphous phase and the crystallization of new phases [45,46], which improved in turn the compressive strength of CTFR at 1050 °C (Fig. 12).

In addition, the absorption band attributed to the vibration of H-O-H bonds in the water molecule and was present at the wavenumber 1650 cm^{-1} in the spectra of both the unheated alkali activated materials in Fig. 17 (a) and 18 (a), respectively, has been eliminated in the spectra of the respective materials exposed to 600 °C (Figs. 17b and 18b).

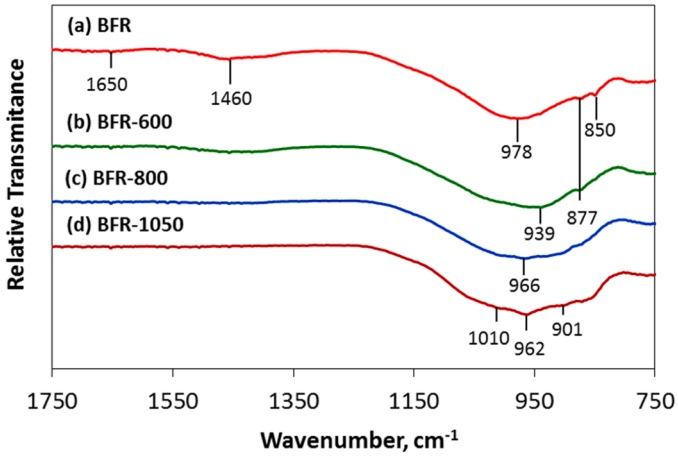

Fig. 17. FTIR spectra of the BFR alkali activated material after (a) curing at 50 °C for 7 d and (b), (c) and (d) exposure for 2 h to 600 °C, 800 °C and 1050 °C, respectively.

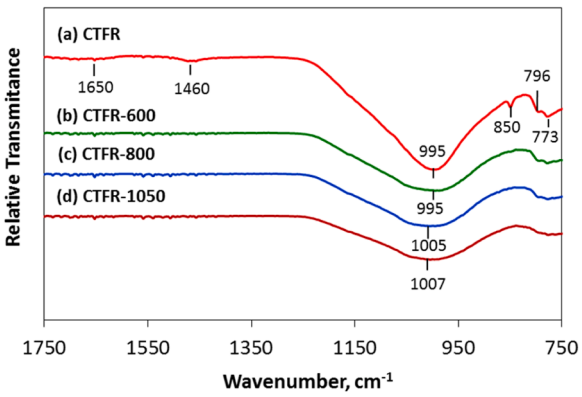

Fig. 18. FTIR spectra of the CTFR alkali activated material after (a) curing at 50 °C for 7 d and (b), (c) and (d) exposure for 2 h to 600 °C, 800 °C and 1050 °C, respectively.

Besides, the peaks related to the C-O-O bond vibrations that appeared at the wavenumbers 1460 cm^{-1} and 877 cm^{-1} in the spectra of both the unheated alkali activated materials, still appeared only in the spectrum of BFR after exposure to 600 °C (Fig. 17b), due to calcite that still existing in BFR at this temperature (Fig. 15b), while it disappeared in all the other spectra of both materials.

4. Conclusions

The present investigation revealed that the mechanical behavior during and after exposure in fire of alkali activated materials based entirely on construction and demolition waste, either waste brick or waste ceramic tiles, allows them to be considered as possible candidates for the passive fire protection of building.

The most prominent findings of this investigation are the following:

The behavior of the studied alkali activated materials, the one based on waste bricks (BFR) and the other based on waste ceramic tiles (CTFR), was totally different in the on-fire and post-fire tests. The differentiations observed in the materials behavior during both types of tests are related to the microstructural transformations occurred in the formed amorphous polymeric aluminosilicate phase.

During the on-fire experiments, BFR behaved as elastic material up to 950 °C, yielding a compressive strength close to the initial value, before its brittle failure, similar to ceramic materials. At 1000 °C, it presented a behavioral variation from linear elastic at the initial stage, where cracks appeared without being spread, to plastic deformation in the following stages, where the relevant specimen was deformed without failing. At 1050 °C, BFR exhibited pseudo-plastic behavior from the test beginning, with plastic deformation of the specimen under negligible mechanical strength, without breaking. On the contrary, the CTFR alkali activated material exhibited plastic behavior from the temperature of 850 °C, undergoing permanent deformation, with signs of melting at the highest tested temperature of 1050 °C.

During the post-fire tests, the BFR geopolymer lost about 20% of its initial compressive strength after its exposure to 600 °C, while after exposure to 800 °C it regained its initial compressive strength, which was slightly increased after exposure to 1050 °C. Accordantly, the CTFR initial compressive strength decreased about 50% after the exposure of CTFR to 600 °C and an additional 10%, after its exposure to 800 °C, while it reached the initial value increased by 10% after the CTFR exposure to 1050 °C.

The dehaydration and dehydroxylation of the amorphous polymeric phase that occurred after the materials' exposure to 600 °C and their subsequent cooling back to ambient temperature, affected the internal porosity and resulted in an extend cracking that decreased importantly their compressive strength. At higher temperatures, around 800 – 900 °C, the polymeric phase was softened ant the formed pseudo-viscous phase filled partially or totally the existing pores and cracks, leading to plastic behavior of the materials in fire conditions and the improvement of their compressive strength after cooling. The heating exposure of the alkali activated materials at temperatures higher than 950 – 1000 °C promoted their plastic behavior. However, after their cooling back to ambient temperature, the sintering phenomena that took place enhanced their mechanical behavior and increased their compressive strength to values higher than the initial ones for both the studied materials.

CRediT authorship contribution statement

Giannopoulou Ioanna: Writing – review & editing, Writing – original draft, Methodology, Data curation, Conceptualization. **Robert Ponsian Mwombeki:** Investigation, Formal analysis. **Petrou Michael:** Investigation. **Nicolaides Demetris:** Supervision, Project administration, Conceptualization.

Declaration of Competing Interest

The authors declare that they have no known competing financial interests or personal relationships that could have appeared to influence the work reported in this paper.

Data Availability

Data will be made available on request.

Acknowledgements

This investigation is performed under the research project entitled "Development of an Innovative Insulation Fire Resistant Façade from the Construction and Demolition Wastes - DEFEAT" (INTEGRATED/0918/0052), which has been co-funded by the European Regional Development Fund (ERDF) and the Cyprus Government, through the RESTART 2016-2020 framework program of the Cyprus Research & Innovation Foundation. The authors kindly acknowledge also (i) Dr. George Vekinis, Research Director in the Laboratory of Advance Ceramics and Composites of the National Center of Scientific Research (NCSR) "DEMOKRITOS" in Athens, Greece, for his cooperation in the performance of the high temperature compression tests of the studied alkali activated materials and (ii) Dr. Theodora Kyratsi, Professor in the Department of Mechanical and manufacturing Engineering at the University of Cyprus for the performance of the X-ray diffraction analyses of the alkali activated materials.

References

[1] I. Fletcher, S. Welch, J. Torero, R. Carvel, A. Usman, Behaviour of Concrete Structures in Fires, J. Therm. Sci. 11 (2007) 37–52, https://doi.org/10.2298/TSCI0702037F.
[2] O. Arioz, Effects of elevated temperatures on properties of concrete, Fire Saf. J. 42 (2007) 516–522, https://doi.org/10.1016/j.firesaf.2007.01.003.
[3] B. Qu, A. Fernandez-Jimenez, A. Palomo, A. Martin, J.Y. Pastor, Effect of high temperatures on the mechanical behavior of hybrid cement, Mater. Constr. 70 (2020) e213, https://doi.org/10.3989/mc.2020.13318.
[4] L. Li, L. Shi, Q. Wang, Y. Liu, J. Dong, H. Zhang, G. Zhang, A review on the recovery of fire-damaged concrete with post-fire-curing, Constr. Build. Mater. 237 (2020) 117564, https://doi.org/10.1016/j.conbuildmat.2019.117564.
[5] J. Davidovits, Geopolymers: ceramic-like inorganic polymers, J. Ceram. Sci. Technol. 8 (3) (2017) 335–350. ⟨http//doi.org/10.4416/JCST2017-00038⟩.
[6] D. Dimas, I. Giannopoulou, D. Panias, Polymerization in sodium silicate solutions: a fundamental process in geopolymerization technology, J. Mater. Sci. 44 (2009) 3719–3730, https://doi.org/10.1007/s10853-009-3497-5.
[7] D. Khale, R. Chaudhary, Mechanism of geopolymerization and factors influencing its development: a review, J. Mater. Sci. 42 (2007) 729–746, https://doi.org/10.1007/s10853-006-0401-4.
[8] M. Zhang, T. El-Korchi, G. Zhang, J. Liang, M. Tao, Synthesis factors affecting mechanical properties, microstructure, and chemical composition of red mud-fly ash based geopolymers, Fuel 134 (2014) 315–325, https://doi.org/10.1016/j.fuel.2014.05.058.

[9] W. Hajjaji, S. Andrejkovicova, C. Zanelli, M. Alshaaer, M. Dondi, J.A. Labrincha, F. Rocha, Composition and technological properties of geopolymers based on metakaolin and red mud, Mater. Des. 52 (2013) 648–654, https://doi.org/10.1016/j.matdes.2013.05.058.
[10] Y. Wu, B. Lu, Z. Yi, F. Du, Y. Zhang, The properties and latest application of geopolymers, IOP Conf. Ser. Mater. Sci. Eng. 472 (2019) 012029, https://doi.org/10.1088/1757-899X/472/1/012029.
[11] P. Duxson, A. Fernandez-Jimenez, J.L. Provis, G.C. Lukey, A. Palomo, J.S.J. van Deventer, Geopolymer technology: the current state of the art, J. Mater. Sci. 42 (2007) 2917–2933, https://doi.org/10.1007/s10853-006-0637-z.
[12] M. Alhawat, A. Ashour, G. Yildirim, A. Aldemir, M. Sahmaran, Properties of geopolymers sourced from construction and demolition waste: a review, J. Build. Eng. 50 (2022) 104104, https://doi.org/10.1016/j.jobe.2022.104104.
[13] H.Y. Zhang, V. Kodur, S.L. Qi, L. Cao, B. Wua, Development of metakaolin–fly ash based geopolymers for fire resistance applications, Constr. Build. Mater. 55 (2014) 38–45.
[14] I. Giannopoulou, D. Panias, I. Maragkos, Synthesis of ferronickel slag-based geopolymers, Miner. Eng. 22 (2009) 196–203, https://doi.org/10.1016/j.mineng.2008.07.003.
[15] Y. Pontikes, L. Machiels, S. Onisei, L. Pandelaers, D. Geysen, P.T. Jones, B. Blanpain, Slags with a high Al and Fe content as precursors for inorganic polymers, Appl. Clay Sci. 73 (2013) 93–102, https://doi.org/10.1016/j.clay.2012.09.020.
[16] T. Bakharev, Thermal behaviour of geopolymers prepared using class F fly ash and elevated temperature curing, Cem. Concr. Res. 36 (6) (2006) 1134–1147, https://doi.org/10.1016/j.cemconres.2004.06.031.
[17] T.W. Cheng, J.P. Chiu, Fire-resistant geopolymer produced by granulated blast furnace slag, Miner. Eng. 16 (2003) 205–210, https://doi.org/10.1016/S0892-6875(03)00008-6.
[18] J. Davidovits, Fire proof geopolymeric cements, in: Proceedings of Second International Conference Geopolymere, 1999, pp. 165–169.
[19] A. Martin, J.Y. Pastor, A. Palomo, A. Fernández Jiménez, Mechanical behaviour at high temperature of alkali-activated aluminosilicates (geopolymers), Constr. Build. Mater. 93 (2015) 1188–1196, https://doi.org/10.1016/j.conbuildmat.2015.04.044.
[20] D. Zaharaki, M. Galetakis, K. Komnitsas, Valorization of construction and demolition (C&D) and industrial wastes through alkali activation, Constr. Build. Mat. 121 (2016) 686–693, https://doi.org/10.1016/j.conbuildmat.2016.06.051.
[21] I. Giannopoulou, P.M. Robert, K.-M. Sakkas, M.F. Petrou, D. Nicolaides, High temperature performance of geopolymers based on construction and demolition waste, J. Build. Eng. 72 (2023) 106575, https://doi.org/10.1016/j.jobe.2023.106575.
[22] V.F.F. Barbosa, K.J.D. MacKenzie, Synthesis and thermal behaviour of potassium sialate geopolymers, Mater. Lett. 57 (9) (2003) 1477–1482, https://doi.org/10.1016/S0167-577X(02)01009-1.
[23] V.F.F. Barbosa, K.J.D. MacKenzie, Thermal behaviour of inorganic geopolymers and composites derived from sodium polysialate, Mater. Res. Bull. 38 (2003) 319–331, https://doi.org/10.1016/S0025-5408(02)01022-X.
[24] P. Duxson, G. Lukey, J.J. van Deventer, Physical evolution of Na-geopolymer derived from metakaolin up to 1000 °C, J. Mater. Sci. 42 (9) (2007) 3044–3054, https://doi.org/10.1007/s10853-006-0535-4.
[25] Y.M. Liew, H. Kamarudin, A.M.M. Al Bakri, M. Bnhussain, M. Luqman, I.K. Nizar, C.M. Ruzaidi, C.Y. Heah, Optimization of solids-to-liquid and alkali activator ratios of calcined kaolin geopolymeric powder, Constr. Build. Mater. 37 (2012) 440–451, https://doi.org/10.1016/j.conbuildmat.2012.07.075.
[26] M. Lahoti, K.H. Tan, E.-H. Yang, A critical review of geopolymer properties for structural fire resistance applications, Constr. Build. Mat. 221 (2019) 514–526, https://doi.org/10.1016/j.conbuildmat.2019.06.076.
[27] G.Y. Kovalchuk, P.V. Krivenko, Producing fire- and heat-resistant geopolymers, in: J.L. Provis, J.S.J. van Deventer (Eds.), Geopolymers Structure, Processing, Properties and Industrial Applications, Woodhead Publishing, 2009, pp. 227–266.
[28] M. Lahoti, K.K. Wong, K.H. Tan, E.-H. Yang, Effect of alkali cation type on strength endurance of fly ash geopolymers subject to high temperature exposure, Mater. Des. 154 (2018) 8–18, https://doi.org/10.1016/j.matdes.2018.05.023.
[29] D. Panias, I. Giannopoulou, Th Perraki, Effect of synthesis parameters on the mechanical properties of fly ash-based geopolymers, Colloids Surf. A Physicochem. Eng. Asp. 301 (2007) 246–254, https://doi.org/10.1016/j.colsurfa.2006.12.064.
[30] P. Rovnanik, P. Bayer, P. Rovnanikova, Characterization of alkali activated slag paste after exposure to high temperatures, Constr. Build. Mater. 47 (2013) 1479–1487, https://doi.org/10.1016/j.conbuildmat.2013.06.070.
[31] K.-M. Sakkas, A. Sofianos, P. Nomikos, D. Panias, Behaviour of fire protection K-geopolymer under successive severe incidents, Materials 8 (9) (2015) 6096–6104, https://doi.org/10.3390/ma8095294.
[32] M. Guerrieri, G.J. Sanjayan, Behaviour of combined fly ash/slag based geopolymers when exposed to high temperatures, Fire Mater. 34 (2010) 163–175, https://doi.org/10.1002/fam.1014.
[33] C.L. Wong, K.H. Mo, S.P. Yap, U.J. Alengaram, T.C. Ling, Potential use of brick waste as alternate concrete-making materials: A review, J. Clean. Prod. 195 (2018) 226–239.
[34] R.A. Robayo-Salazar, R.A. Rivera, J.F. de Gutiérrez, R.M, Alkali-activated building materials made with recycled construction and demolition wastes, Constr. Build. Mater. 149 (2017) 130–138, https://doi.org/10.1016/j.conbuildmat.2017.05.122.
[35] K. Komnitsas, D. Zaharaki, A. Vlachou, G. Bartzas, M. Galetakis, Effect of synthesis parameters on the quality of construction and demolition wastes (CDW) geopolymers, Adv. Powder Technol. 26 (2015) 368–376, https://doi.org/10.1016/j.apt.2014.11.012.
[36] D. Kioupis, A. Skaropoulou, S. Tsivilis, G. Kakali, Valorization of brick and glass CDWs for the development of geopolymers containing more than 80% of wastes, Minerals (2020), https://doi.org/10.3390/min10080672.
[37] A.R.G. Azevedo, C.M.F. Vieira, W.M. Ferreira, K.C.P. Faria, L.G. Pedroti, B. C. Mendes, Potential use of ceramic waste as precursor in the geopolymerization reaction for the production of ceramic roof tiles, J. Build. Eng. 29 (2020) 101156, https://doi.org/10.1016/j.jobe.2019.101156.
[38] European Commission, Development and Implementation of Initiatives Fostering Investment and Innovation in Construction and Demolition Waste Recycling Infrastructure, Publications Office of the European Union, 2018. https://doi.org/10.2873/11837.
[39] M. Behera, S.K. Bhattacharyya, A.K. Minocha, R. Deoliya, S. Maiti, Recycled aggregate from C&D waste & its use in concrete – a breakthrough towards sustainability in construction sector: A review, Constr. Build. Mater. 68 (2014) 501–516.
[40] Y.M. Liew, H. Kamarudin, A.M.M. Al Bakri, M. Bnhussain, M. Luqman, I.K. Nizar, C.M. Ruzaidi, C.Y. Heah, Optimization of solids-to-liquid and alkali activator ratios of calcined kaolin geopolymeric powder, Constr. Build. Mater. 37 (2012) 440–451, https://doi.org/10.1016/j.conbuildmat.2012.07.075.
[41] K.G. Knauss, T.J. Wolery, Dependence of albite dissolution kinetics on ph and time at 25°C and 70°C, Geochem. Cosmochim. Acta 50 (11) (1986) 2481–2497, https://doi.org/10.1016/0016-7037(86)90031-1.
[42] C. Kosanovic, S. Bosnar, B. Subotic, V. Svetlicic, T. Misic, G. Drazic, K. Havancsak, Study of the microstructure of amorphous aluminosilicate gel before and after its hydrothermal treatment, Micro Mesopor. Mat. 110 (2008) 177–185, https://doi.org/10.1016/j.micromeso.2007.06.007.
[43] I. Giannopoulou, D. Panias, Hydrolytic stability of sodium silicate gels in the presence of aluminum, J. Mater. Sci. 45 (2010) 5370–5377, https://doi.org/10.1007/s10853-010-4586-1.
[44] G. Yuan, Y. Cao, H.-M. Schulz, F. Hao, J. Gluyas, K. Liu, T. Yang, Y. Wang, K. Xi, F. Li, A review of feldspar alteration and its geological significance in sedimentary basins: from shallow aquifers to deep hydrocarbon reservoirs, Earth Sci. Rev. 191 (2019) 114–140, https://doi.org/10.1016/j.earscirev.2019.02.004.
[45] A. Fernandez-Jimenez, A. Palomo, Mid-infrared spectroscopic studies of alkali activated fly ash structure, Microporous Mesoporous Mater. 86 (2005) 207–214, https://doi.org/10.1016/j.micromeso.2005.05.057.
[46] A. Rees, J.L. Provis, G.C. Lukey, J.S.J. van Deventer, Attenuated total reflectance Fourier Transform infrared analysis of fly ash geopolymer gel aging, Langmuir 23 (2007) 8170–8179, https://doi.org/10.1021/la700713g.
[47] G. Cultrone, I. Sidraba, E. Sebastian, Mineralogical and physical characterization of the bricks used in the construction of the "Triangul Bastion", Riga (Latvia), Appl. Clay Sci. 28 (2005) 297–308, https://doi.org/10.1016/j.clay.2004.02.005.
[48] J.S.J. Van Deventer, J.L. Provis, P. Duxson, G.C. Lukey, Reaction mechanisms in the geopolymeric conversion of inorganic waste to useful products, J. Hazard. Mater. 139 (2007) 506–513, https://doi.org/10.1016/j.jhazmat.2006.02.044.
[49] R. Ahmad, W.M.W. Ibrahim, M.M.A.B. Abdullah, P. Pakawanit, P. Vizureanu, A. S. Abdullah, A.V. Sandu, F.H. Ahmad Zaidi, Geopolymer-based nepheline ceramics: effect of sintering profile on morphological characteristics and flexural strength, Crystals 12 (2022) 1313, https://doi.org/10.3390/cryst12091313.
[50] I.C. Minota-Yepes, R. Alvarez-Roca, F.A. Londono-Badillo, Review: densification process of ceramic materials, Respuestas 25 (2020) 199–212, https://doi.org/10.22463/0122820X.2964.